REGION-SPECIFIC METABOLIC ALTERATIONS IN BRAIN OF THE APP/PS1 TRANSGENIC MICE OF ALZHEIMER'S DISEASE

Raúl González-Domínguez[a,b,c], Tamara García-Barrera[a,b,c], Javier Vitorica[d,e,f], José Luis Gómez-Ariza[a,b,c]

[a]Department of Chemistry and CC.MM. Faculty of Experimental Sciences. University of Huelva. Campus de El Carmen. 21007 Huelva. SPAIN; [b]Campus of Excellence International ceiA3. University of Huelva. SPAIN; [c]Research Center of Health and Environment (CYSMA). University of Huelva. Campus de El Carmen. 21007 Huelva. SPAIN; [d]Department Bioquímica, Bromatologia, Toxicología y Medicina Legal, Faculty of Pharmacy, University of Seville. 41012 Seville. SPAIN, [e]Centro de Investigación Biomédica en Red sobre Enfermedades Neurodegenerativas (CIBERNED). 41013 Seville. SPAIN, [f]Instituto de Biomedicina de Sevilla (IBiS)–Hospital Universitario Virgen del Rocío/CSIC/University of Seville. 41013 Seville. SPAIN

e-mail addresses: raul.gonzalez@dqcm.uhu.es, tamara.garcia@dqcm.uhu.es, vitorica@us.es, ariza@uhu.es

Corresponding authors:
Prof. J.L Gómez-Ariza, Tel.: +34 959 219968, fax: +34 959 219942, e-mail: ariza@uhu.es
Dr. T. García-Barrera, Tel.: +34 959 219962, fax: +34 959 219942, e-mail: tamara@dqcm.uhu.es

ABSTRACT
Alzheimer's disease (AD) is the most common neurodegenerative disorder worldwide, but its etiology is still not completely understood. The identification of underlying pathological mechanisms is becoming increasingly important for the discovery of biomarkers and therapies, for which metabolomics presents a great potential. In this work, we studied metabolic alterations in different brain regions of the APP/PS1 mice by using a high-throughput metabolomic approach based on the combination of gas chromatography-mass spectrometry and ultra-high performance liquid chromatography-mass spectrometry. Multivariate statistics showed that metabolomic perturbations are widespread, affecting mainly to hippocampus and cortex, but also present in regions not primarily associated with AD such as striatum, cerebellum and olfactory bulbs. Multiple metabolic pathways could be linked to the development of AD-type disorders in this mouse model, including abnormal purine metabolism, bioenergetic failures, dyshomeostasis of amino acids and disturbances in membrane lipids, among others. Interestingly, region-specific alterations were observed for some of the potential markers identified, associated with abnormal fatty acid composition of phospholipids and sphingomyelins, or differential regulation of neurotransmitter amino acids (e.g. glutamate, glycine, serine, N-acetyl-aspartate), not previously described to our knowledge. Therefore, these findings could provide a new insight into brain pathology in Alzheimer's disease.

KEYWORDS
Metabolomics, APP/PS1 mice, Alzheimer's disease, region-specific alterations, pathology

ABBREVIATIONS
AD: Alzheimer's disease; GC-MS: gas chromatography mass spectrometry; UPLC-MS: ultra-high performance liquid chromatography mass spectrometry; APP: amyloid precursor protein; PS1: presenilin 1; TG: transgenic; WT: wild type; QC: quality control; PCA: principal component analysis; PLS-DA: partial least squares discriminant analysis; VIP: variable importance in the projection.

1. Introduction

Alzheimer's disease (AD) is the most common neurodegenerative disorder among older people, which involves a progressive loss of memory and cognitive abilities leading to dementia. Deposition of senile plaques containing β-amyloid peptides and formation of neufibrillary tangles are the two major hallmarks of AD (Selkoe 2003), but other profound biochemical alterations also occur in the AD brain, including oxidative stress, mitochondrial, dysfunction, inflammation, membrane lipid dysregulation and neurotransmitter disruption, among others (Maccioni *et al.* 2001; Maruszak and Zekanowski 2011; Kosicek and Hecimovic 2013). These pathological lesions are mainly localized in medial temporal lobe structures, specifically the cortex and hippocampus (Braak and Braak 1991), contributing to neuronal degeneration, loss of synapses, and brain atrophy. However, it has been demonstrated that perturbations are more widespread and affect to a variety of sites such as cerebellum (Braak *et al.* 1989), brainstem (Simic *et al.* 2009) or the olfactory system (Struble and Clark 1992). Neuroimaging techniques have been extensively applied for *in vivo* detection of neuropathological features in AD patients, including magnetic resonance imaging (MRI) to measure structural and functional changes of brain (Lin *et al.* 2012), positron emission tomography (PET) for detection of amyloid plaques (Rowe and Villemagne 2013) and changes in glucose metabolism (Mosconi *et al.* 2009), and magnetic resonance spectroscopy (MRS) to quantify metabolite markers (Kantarci *et al.* 2007). On the other hand, metabolomic analysis is gaining great importance for the discovery of novel potential biomarkers for diagnosis and the elucidation of underlying mechanisms. Metabolomics, based on the comprehensive and simultaneous analysis of multiple metabolites in biological samples, presents a great potential in health survey for the study of disease pathology, discovery of biomarkers and drug development because metabolites represent the end point of biological reactions, reflecting well the interactions between genes, proteins and the environment (Lindon *et al.* 2004). Thereby, several metabolomic studies have been performed in the last years for the investigation of AD (Ibáñez *et al.* 2013). Most of these studies have been performed in biofluids due to the difficult availability of human brain tissue, and because the use of postmortem tissues supposes that disease is at its end stage. Thus, only a few preliminary studies have been previously reported in this subject (Botosoa *et al.* 2012; Inoue *et al.* 2013; Graham *et al.* 2013a), demonstrating the potential of this approach although requires further investigation with larger and better characterized patient cohorts. Alternatively, numerous transgenic animal models have been developed for studying AD pathophysiology (Hall and Roberson 2012), from which brain samples can be obtained at different stages of disease. Forster et al. used the TASTPM transgenic mice to investigate brain longitudinal metabolic differences by proton magnetic resonance spectroscopy, and found significant differences in levels of metabolites such as myo-inositol, succinate, glycerophosphocholine and choline (Forster *et al.* 2011). In other studies, the metabolic profiles of both brain and plasma from different mouse models were characterized and compared to those from wild-type mice (Hu *et al.* 2012; Graham *et al.* 2013b). Lower levels of metabolites were found in plasma samples, and they fluctuate more between the two groups than brain metabolites. However, the statistical models built using plasma metabolite profiles were more accurate than brain tissue despite the smaller number of factors. Furthermore, the role of a dysregulated endocannabinoid-eicosanoid network in pathogenesis of AD has been recently demonstrated in the APP/PS1 mice with inactivated monoacylglycerol lipase (Piro *et al.* 2012). On the other hand, other studies focused on individual brain areas including hippocampus (Trushina *et al.* 2012; Lin *et al.* 2013; Wang *et al.* 2014), cortex (Dedeoglu *et al.* 2004) and cerebellum (Lin *et al.* 2014; Balayssac *et al.* 2013), because metabolic perturbations induced by AD-type disorders could be region-specific in the brain. In this sense, the characterization of regional metabolomic perturbations may be of greater interest in order to investigate the impact of disease on different brain regions and determine the most affected ones in AD mice. Only a few authors have previously performed a comparative metabolomic investigation in different brain areas, by using *in vitro* nuclear magnetic resonance (Salek *et al.* 2010; Woo *et al.* 2010; Lalande *et al.* 2014). These findings demonstrated that hippocampus and cortex are the most sensitive regions during early-stage AD, but perturbations in metabolism also affect other tissues such as cerebellum and midbrain. However, limited metabolic information was obtained considering the total number of discriminant metabolites detected (N-acetylaspartate, myoinositol, glutamate, GABA, creatine, taurine, and a few others), because of the low sensitivity of this approach. For this reason, the application of high-throughput metabolomic approach based on mass spectrometry could be of great interest in order to delve into metabolic alterations associated with Alzheimer's disease occurring in different brain regions.

In this study, a metabolomic platform based on complementary analysis by gas chromatography-mass spectrometry (GC-MS) and reversed-phase ultra-high performance liquid chromatography-mass

spectrometry (UPLC-MS) was used to investigate metabolic perturbations in five brain regions of the APP/PS1 transgenic mice of Alzheimer's disease, including cortex, hippocampus, striatum, cerebellum and olfactory bulbs. This mouse model is extensively employed in AD research given that reproduces well some of the neuropathological and cognitive deficits observed in human Alzheimer, with a phenotype characterized by deposition of Aβ plaques starting from the age of four months, glial activation, and deficits in cognitive functions at the age of 6 months (Malm *et al.* 2011). Furthermore, the application of this multiplatform approach using two complementary methods allowed extending the analytical coverage of endogenous metabolites present in brain samples compared with conventional procedures based on NMR. Thereby, while GC-MS provides high-chromatographic resolution for primary low molecular weight metabolites, reversed phase liquid chromatography can be considered as the standard tool for the separation of medium polar and non-polar analytes. Multivariate statistics was used to discriminate metabolic profiles from transgenic animals and wild-type controls, and thus numerous metabolites could be identified as potential markers of disease. These findings indicated that all brain regions analyzed are affected to a greater or lesser extent, but in addition it is noteworthy that some of these metabolic alterations could be region-specific.

2. Materials and methods

2.1. Animal handling

Transgenic APP/PS1 mice (C57BL/6 background) were generated as previously described by Jankowsky et al., expressing the Swedish mutation of APP together with PS1 deleted in exon 9 (Jankowski *et al.* 2004). On the other hand, age-matched wild-type mice of the same genetic background (C57BL/6) were purchased from Charles River Laboratory for their use as controls (WT). In this study, male and female animals at 6 months of age were used for experiments (TG: N=30, male/female 13/17; WT: N=30, male/female 15/15). Animals were acclimated for 3 days after reception in rooms with a 12-h light/dark cycle at 20-25 °C, with water and food available *ad libitum*. Then, mice were anesthetized by isoflurane inhalation and sacrificed by exsanguination via cardiac puncture. Brains were rapidly removed, rinsed with saline solution (0.9% NaCl w/v) and dissected into hippocampus, cortex, striatum, cerebellum and olfactory bulbs. Finally, tissues were transferred to individual Eppendorf tubes, snap-frozen in liquid nitrogen and stored at −80 °C until analysis. Animals were handled according to the directive 2010/63/EU stipulated by the European Community, and the study was approved by the Ethical Committee of University of Huelva.

2.2. Sample preparation

Large brain regions (cortex and cerebellum) were cryo-homogenized using a cryogenic homogenizer SPEX SamplePrep (Freezer/Mills 6770), during 30 seconds at rate of 10 strokes per second. Subsequently, tissues were extracted with pre-cooled 0.1% formic acid in methanol (-20ºC) using a pellet mixer for cell disruption (VWR International, UK). For this, tissue samples were exactly weighed in Eppendorf tubes (30 mg for homogenized tissues, and the entire organ for smaller tissues) and mixed with the extraction solvent (10 µl/mg). The mixture was homogenized during 2 min in an ice bath, and then centrifuged at 10000 g for 10 min at 4ºC. An aliquot of the supernatant (50 µl) was splitted for derivatization before GC-MS fingerprinting, and the rest of the sample was transferred to the injection vial for UPLC-MS analysis. Derivatization was carried out according to a two-step methodology previously described (Begley *et al.* 2009). For this, 50µl of extracts were dried under nitrogen stream and redissolved in 50 µL of 20 mg mL^{-1} methoxyamine in pyridine for protection of carbonyl groups by methoximation. After briefly vortexing, samples were incubated at 80°C for 15 min in a water bath. Then silylation was performed by adding 50 µL of MSTFA and incubating at 80°C for a further 15 min. Finally, extracts were centrifuged at 4000 g for one minute and supernatant was collected for analysis. Furthermore, quality control (QC) samples were prepared by pooling equal volumes of each sample, which allows monitoring the stability and performance of the system along the analysis period (Sangster *et al.* 2006).

2.3. Metabolomic analysis by GC-MS

Analyses were performed in a Trace GC ULTRA gas chromatograph coupled to an ion trap mass spectrometer detector ITQ 900 (Thermo Fisher Scientific), using a Factor Four capillary column VF-5MS 30m×0.25mm ID, with 0.25 µm of film thickness (Varian). The GC column temperature was set to 100ºC for 0.5 minutes, and programmed to reach 320ºC at a rate of 15ºC per minute. Finally, this temperature was maintained for other 2.8 minutes, being the total time of analysis 18 minutes. The injector temperature was kept at 280ºC, and helium was used as carrier gas at a constant flow rate of 1 ml min^{-1}. For mass spectrometry detection, ionization was carried out by electronic impact (EI) using a voltage of

70 eV, and the ion source temperature was set at 200ºC. Data were obtained acquiring full scan spectra in the m/z range 35-650. For analysis, 1 µl of sample is injected in splitless mode.

2.4. Metabolomic analysis by UPLC-MS

Samples were fingerprinted by ultra performance liquid chromatography (Accela LC system, Thermo Fisher Scientific) coupled to a quadrupole-time-of-flight mass spectrometry system equipped with electrospray source (QSTAR XL Hybrid system, Applied Biosystems). Chromatographic separations were performed in a reversed-phase column (Hypersil Gold C18, 2.1x50 mm, 1.9µm) thermostated at 50ºC, with an injection volume of 5µl. Solvents were delivered at a flow rate 0.5ml/min, using methanol (solvent A) and water (solvent B), both containing 10mM ammonium formate and 0.1% formic acid. The gradient elution program was: 0-1 min, 95% B; 2.5 min, 25% B; 8.5-10 min, 0% B; 10.1-12 min, 95% B. MS operated in positive and negative polarities, acquiring full scan spectra in the m/z range 50-1000 with 1.005 seconds scan time. The ion spray voltage (IS) was set at 5000V and -2500V, and high-purity nitrogen was used as curtain, nebulizer and heater gas at flow rates about 1.48 L min^{-1}, 1.56 L min^{-1} and 6.25 L min^{-1}, respectively. The source temperature was fixed at 400ºC, with a declustering potential (DP) of 100V/-120V, and a focusing potential (FP) of ±350V. To acquire MS/MS spectra, nitrogen was used as collision gas.

2.5. Data pre-processing

Raw data was processed following the pipeline described by Katajamaa et al., which proceeds through multiple stages including feature detection, alignment of peaks and normalization (Katajamaa and Oresic 2007). For this purpose, we employed the freely available software XCMS, included in the R platform (http://www.r-project.org). UPLC-MS files were converted into mzXML format using the msConvert tool (ProteoWizard), while GC-MS files were converted into netCDF using the Thermo File Converter tool (Thermo Fisher Scientific). Subsequently, data were extracted using the matchedFilter method. This algorithm slices data into extracted ion chromatograms (XIC) on a fixed step size (default 0.1 m/z), and then each slice is filtered with matched filtration using a second-derivative Gaussian as the model peak shape (Smith *et al.* 2006). The XCMS parameters were optimized according to the characteristics of data sets obtained in order to extract the maximum information as possible. Finally, the settings applied for UPLC-MS data were S/N threshold 2 and full width at half-maximum (fwhm) 10, while for GC-MS data the fwhm was set at 3. After peak extraction, grouping and retention time correction of peaks (alignment) was accomplished in three iterative cycles with descending bandwidth (bw) from 10 to 1 seconds in UPLC-MS, and descending bw from 5 to 1 seconds for GC-MS. Then, imputation of missing values was performed by returning to the raw spectral data and integrating the areas of the missing peaks which are below the applied signal-to-noise ratio threshold, using the fillPeaks algorithm. For data normalization, the locally weighted scatter plot smoothing (LOESS) normalization method was used, which adjusts the local median of log fold changes of peak intensities between samples in the data set to be approximately zero across the whole peak intensity range (Veselkov *et al.* 2011). Finally, data were submitted to logarithmic transformation, in order to stabilize the variance of results. The preprocessed data were then exported as a .csv file for further data analysis by multivariate procedures.

2.6. Multivariate statistics

Data were subjected to multivariate analysis by principal component analysis (PCA) and partial least squares discriminant analysis (PLS-DA) in order to compare metabolomic profiles obtained, using the SIMCA-P™ software (version 11.5, UMetrics AB, Umeå, Sweden). Before performing statistical analysis, data was submitted to Pareto scaling for reducing the relative importance of larger values (van den Berg *et al.* 2006). Quality of the models was assessed by the R^2 and Q^2 values, supplied by the software, which provide information about the class separation and predictive power of the model, respectively. These parameters are ranged between 0 and 1, and they indicate the variance explained by the model for all the data analyzed (R^2) and this variance in a test set by cross-validation (Q^2). Finally, potential biomarkers were selected according to the Variable Importance in the Projection, or VIP (a weighted sum of squares of the PLS weight, which indicates the importance of the variable in the model), considering only variables with VIP values higher than 1.5, indicative of significant differences among groups. Furthermore, these metabolites were validated by t-test with Bonferroni correction for multiple testing (p-values below 0.05), using the STATISTICA 8.0 software (StatSoft, Tulsa, USA).

2.7. Metabolites identification

Discriminant metabolites detected by GC-MS were identified using the NIST Mass Spectral Library (version 08), considering only those variables with a similarity index (SI) greater than 70%. Alternatively, identification of metabolites from UPLC-MS profiling was made matching the experimental accurate

mass and tandem mass spectra (MS/MS) with those available in metabolomic databases (HMDB, METLIN and LIPIDMAPS). Furthermore, identity of lipids was confirmed based on characteristic fragmentation patterns previously described. Phosphatidylcholines (PCs) and lysophosphatidylcholines (LPCs) presented characteristic ions in positive ionization mode at m/z 184, 104 and 86, and two typical fragments due to the loss of trimethylamine (m/z 59) and phosphocholine (m/z 183). In contrast, the product-ion spectra of ethanolamines and serines were dominated by $[M+H-141]^+$ and $[M+H-185]^+$ respectively, arising from the elimination of the phosphoethanolamine or phosphoserine moiety. Finally, in negative mode these distinctive signals were found at 168, 196, 241, 171 and $[M-H-87]^-$, for choline, ethanolamine, inositol, glycerol and serine derived lipids, respectively (Pulfer and Murphy 2003). Furthermore, the fragmentation in the glycerol backbone and release of the fatty acyl substituents enabled the identification of individual species of phospholipids, as previously described (Wang *et al.* 2004). For sphingomyelins, typical product ions appear at m/z 264 and 282 due to the fragmentation in the sphingosine moiety, and the cleavage of phosphocholine headgroup generates characteristic fragments at 184 and 168 m/z, in positive and negative modes respectively (Haynes *et al.* 2009).

3. Results

Metabolomic profiles corresponding to transgenic animals, wild-type controls and quality control samples were aligned together to perform sample classification by multivariate data analysis. An initial principal components analysis (PCA) plot was generated with data from each brain region using the different techniques (UPLC-ESI(+)/MS, UPLC-ESI(-)/MS, GC-MS) in order to check trends, outliers and quality of the analysis, and to ensure grouping of QC samples. A good clustering of quality control samples was observed in the scores plot (Fig 1A, for hippocampus), indicative of stability during the analyses (Sangster *et al.* 2006), without significant outliers according to the Hotelling T^2-range plot (not shown). Partial least squares discriminant analysis (PLS-DA) was used in the same data sets to obtain a perfect separation of the different study groups (Fig 1B, for hippocampus). These models yielded satisfactory values for the quality parameters R^2 and Q^2, with a variance explained close to 100% and variance predicted above 60% for all models (Table 1).

Discriminant metabolites were then selected according to the VIP value for each PLS-DA model (Tables 2-4). Major changes were observed in amino acids and related compounds, nucleotides, and other low molecular weight metabolites (Table 2), lysophospholipids (Table 3) and phospholipids (Table 4). Most of these metabolomic alterations were found in hippocampus and cortex, but several impairments were also present in cerebellum, striatum and olfactory bulbs. Moreover, it is noteworthy that some metabolites showed opposite trends in different brain areas, suggesting that region-specific perturbations might occur. Therefore, the characterization of regional metabolic abnormalities in brain of the APP/PS1 mice might provide an interesting insight into pathological mechanisms associated with the development and spread of disease in brain.

4. Discussion

A metabolomic platform based on the combination of gas chromatography-mass spectrometry and reversed-phase ultra-high performance liquid chromatography-mass spectrometry was used to study regional metabolic abnormalities in brain of 6 months-old APP/PS1 transgenic mice. This mouse model, co-expressing mutated amyloid precursor protein and deleted presenilin 1, exhibits accelerated AD phenotype characterized by amyloid deposits and behavioral deficits (Malm *et al.* 2011). Furthermore, the study of the neurochemical profile and age-dependent metabolic changes exhibited by the transgenic APP/PS1 mice has demonstrated that these alterations precede cognitive dysfunctions (Chen *et al.* 2012), being very similar to those found in human Alzheimer's disease. Therefore, the characterization of region-specific metabolic abnormalities in this model might aid in the investigation of the pathological mechanisms associated with AD.

Purine metabolism has been repeatedly associated with neurodegenerative mechanisms occurring in Alzheimer's disease, which is in accordance with our metabolomic findings (Table 2). Hippocampus was the most affected region, but these metabolic changes were also observed in other areas such as cortex, striatum and cerebellum (in this order). Cyclic nucleotides, cyclic adenosine monophosphate (cAMP) and cyclic guanosine monophosphate (cGMP), are second messengers associated with neuroplasticity and neuroprotection, which have been suggested to be affected in AD. Phosphodiesterases, enzymes responsible for the breakdown of cyclic nucleotides, appear to be over-expressed in AD brains (Bolle and Prickaerts 2012), together with a perturbation of cAMP/PKA (Liang *et al.* 2007) and NO/cGMP (Domek-Lopacinska and Strosznajder 2010) signaling pathways, supporting the decrease of these compounds in brain tissue (Table 2). On the other hand, reduced levels of adenosine monophosphate (AMP) could be related to accelerated degradation due to elevated activity of adenosine monophosphate deaminase in brain, provoking over-production of ammonia leading to hyperammonemia (Sims *et al.* 1998). This

decrease of AMP levels may have important consequences in cellular energy homeostasis, given that it plays a central role in glucose and lipid metabolism through the AMP-activated protein kinase (AMPK), which is known to be decreased in AD brain (Cai *et al.* 2012). Concentrations of nucleosides (adenosine, guanosine, inosine) tended to be higher in brains from APP/PS1 mice, which might suggest a disturbed neuroprotective function leading to neural damage because purine nucleosides exert important neuromodulator roles in the central nervous system (Thauerer *et al.* 2012). In addition, this abnormal recycling of brain nucleosides is finally reflected in altered levels of other purine metabolites such as adenine, hypoxanthine and xanthine (Table 2), in agreement with previous studies (Lin *et al.* 2014; Kaddurah-Daouk *et al.* 2011, 2013). Therefore, metabolism of purines highlights as a candidate pathway for the search of potential markers of pathological processes occurring in the APP/PS1 transgenic mice, as schematized in Fig. 2 (simplified scheme of biochemical pathways related to metabolism of purines according to the Kyoto Encyclopedia of Genes and Genomes).

Homeostasis of amino acids also suffered important impairments in brain of the APP/PS1 transgenic mice. Glutamate and glycine were reduced in hippocampus and cortex, while hippocampal serine was increased, denoting a dysfunctional modulation of N-methyl-D-aspartate receptors (NMDA-R). In this sense, it has been reported that NMDA receptors are decreased in different areas of brain with AD (Mota *et al.* 2014), resulting in reduced levels of agonist neurotransmitter amino acids such as glutamate (Wang *et al.* 2014; Salek *et al.* 2010; Lalande *et al.* 2014), glycine (Wang *et al.* 2014) and D-serine, this latter accompanied with increased L-serine (Hu *et al.* 2012; Hashimoto *et al.* 2004). By contrast, the opposite trend was observed in cerebellum, with increased levels of glutamate and glycine (Table 2). This could be because NMDA receptors have specific characteristics in cerebellum that make their function and modulation different from those of NMDA receptors in other brain areas (Llansola *et al.* 2005). Thereby, Balayssac et al. found a significant increase of cerebellar glutamate in the APP-Tg2576 transgenic mice (Balayssac *et al.* 2013), confirming a differential dysregulation of NMDA synapse depending on the brain region considered. Finally, striatum showed a significant increase of glutamate levels, as observed in cerebellum, but alterations of other NMDA co-agonists (glycine and serine) were in line with what described for hippocampus and cortex. Therefore, it could be concluded that region-specific alterations occur in NMDA signaling, which has not been described in any previous metabolomic study of AD, demonstrating the specificity of pathological mechanisms in brain of the APP/PS1 transgenic mice. Moreover, this abnormal content of brain amino acids could also indicate a deregulation of their transport across the blood brain barrier, supported by altered pyroglutamate levels. Amino acids enter into the central nervous system by means of the sodium-independent system L1 regulated by the γ-glutamyl cycle (Lee *et al.* 1996). In this process, amino acids react with glutathione by the action of γ-glutamyl transpeptidase to form γ-glutamyl amino acids, which after enter cells are degraded to the corresponding amino acid, being liberated a molecule of pyroglutamate that is essential since stimulates sodium dependent carriers for the later removal of deleterious amino acids from brain. In this context, reduced levels of pyroglutamate have been previously reported in AD brain (Trushina *et al.* 2012), as observed in hippocampus, cortex, and striatum (Table 2). However, pyroglutamate was increased in cerebellum, in accordance with the specific alterations observed in this region regarding glutamate and glycine. Similarly to glutamate, aspartate is an excitatory neurotransmitter that usually presents lower concentrations in AD brain (Wang *et al.* 2014). Interestingly, levels of this amino acid were reduced in brain regions where glutamate was decreased (hippocampus, cortex and olfactory bulbs), pointing to correlated metabolic networks. In the same way, a similar correlation was observed between levels of glutamate and N-acetylaspartate (NAA). This neurochemical is a conventional biomarker for neuronal integrity whose reduction has been traditionally associated with neural loss in Alzheimer's disease (Salek *et al.* 2010; Lalande *et al.* 2014), in agreement with our metabolomic results in hippocampus, cortex and olfactory bulbs (Table 2). By contrast, striatal and cerebellar levels of NAA were higher in the APP/PS1 mice, which could be linked to increased glutamate through the destabilization of Ca^{2+} homeostasis, as previously described for cerebellum of the APP-Tg2576 model (Balayssac *et al.* 2013) Taurine is an amino acid highly concentrated in rodent brain, with several roles in neurotransmission, neuromodulation, osmoregulation, control of calcium influx, and cell excitability. In this study, we observed a slight decrease in its concentration in all brain regions investigated (except for olfactory bulbs), in accordance with a previous metabolomic study (Salek *et al.* 2010). On the other hand, threonine connects the metabolism of glycine and serine to biosynthesis of branched-chain amino acids, so hippocampal deficiency of this amino acid might be correlated with perturbations in levels of glycine, serine and valine (Table 2). Finally, reductions in histidine and its precursor, phosphoribosyl-AMP, might suggest impaired synthesis of carnosine and/or histamine, important biomolecules associated with oxidative stress (Hipkiss 2007) and failures in neurotransmission (Nuutinen and Panula 2010) in Alzheimer's disease.

Metabolomic signatures also revealed significant disturbances in energy metabolism, principally in hippocampus and cortex, considering decreased levels of lactic acid, malic acid, creatinine, 2-

hydroxyglutaric acid, pyrophosphate (PPi), citric acid ad glucose-6-phosphate (G6P), as well as increased lactose (Table 2). The decrease of glycolytic intermediates (lactate and G6P) and increased lactose levels support a reduced carbohydrate metabolism, while reduced citrate (in all brain regions studied) and malate (only in hippocampus and cortex) could be behind perturbed Krebs cycle, in agreement with previous studies (Hu *et al.* 2012; Trushina *et al.* 2012; Wang *et al.* 2014; Redjems-Bennani *et al.* 1998). Reduced PPi, formed by the hydrolysis of ATP into AMP, denoted mitochondrial impairments related to aberrations in the oxidative phosphorylation system. Moreover, the deficiency of 2-hydroxyglutarate also points to disrupted mitochondrial activity, given that this compound is a byproduct resulting from a side-reaction of malate dehydrogenase (Van Schaftingen *et al.* 2009). Furthermore dyshomeostasis of phosphocreatine system might also occur in brain, considering the decrease of creatinine levels observed in all brain regions analyzed. Therefore, it could be concluded that defects in energy metabolism are a key hallmark in the APP/PS1 transgenic mice of AD, involving multiple metabolic pathways such as glycolysis, TCA cycle, oxidative phosphorylation or phosphocreatine system.

Numerous alterations were also observed in metabolism of phospholipids, as reflected in Tables 2-4, which depended on the type of fatty acid linked to the molecular moiety. Phospholipids containing polyunsaturated fatty acids (principally docosahexaenoic acid) were reduced in brain samples, including phosphatidylcholines (mainly in cortex and striatum) and minor species such as phosphatidylserines, phosphatidylinositols and phosphatidylglycerols (in hippocampus and to a lesser extent cortex). Furthermore, most phospatidylethanolamines and plasmenylethanolamines were decreased as well, principally in hippocampus but also affecting other areas investigated. These deficits in certain phospholipids suggest a role for oxidative stress in the increased degradation of these compounds, in accordance with previous studies in brain from transgenic mice of AD (Yao *et al.* 2009; Han *et al.* 2001; Chan *et al.* 2012). By contrast, a parallel accumulation of phospholipids containing short chain fatty acids was also observed, especially in phosphocholines and phosphoserines from hippocampus and cortex (Table 4). Thereby, membrane destabilization processes in the APP/PS1 mice could be related to imbalances in the levels of saturated/unsaturated fatty acids contained in the structure of phospholipids, as recently proposed for human AD (González-Domínguez *et al.* 2014a). Moreover, phospholipids derived from docosapentaenoic and docosatetraenoic acids were also increased in cortex and other brain regions (Table 4), which might be correlated to peroxisomal dysfunction given that these fatty acids are intermediates for the biosynthesis of DHA and other long chain polyunsaturated fatty acids in peroxisomes. Surprisingly, aforementioned changes were accompanied by an overall increase of arachidonoyl-derived phospholipids (i.e. stearoyl-arachidonoyl phospholipids and di-arachidonoyl phospholipids), being cortex the most affected region. This altered fatty acid profile could suggest a deregulation in the biosynthesis, turnover and acyl chain remodeling of phospholipids, with a great relevance in AD pathology given that the release and oxidation of arachidonic acid from these phospholipids may produce several lipid mediators closely associated with neuronal pathways involved in AD (Frisardi *et al.* 2011). Besides these changes in phospholipid species, numerous byproducts resulting from their degradation were found in brain of the APP/PS1 mice. Thereby, hydrolysis of the ester bonds from phospholipids by the action of PLA_2 leads to the accumulation of brain lysophospholipids (Table 3), not previously described to our knowledge in the APP/PS1 mice. In addition, catabolic metabolites glycerophosphocholine, phosphocholine and choline were elevated, in agreement with previous reports (Walter *et al.* 2004), as well as the final products of this degradation process, glycerol-3-phosphate and free glycerol (Table 2). On the other hand, biosynthesis of phosphatidylcholines via the Kennedy cycle was also disturbed in hippocampus, considering reductions in the precursor uridine monophosphate (Czech *et al.* 2012). Furthermore the decrease of ethanolamine, involved in the turnover of phosphatidylethanolamines, has been previously observed in postmortem AD brains (Ellison *et al.* 1987), corroborating the evidence for a membrane defect in Alzheimer disease.

Alternatively, alterations in sphingomyelins (Table 4) and cholesterol (Table 2) also emerge as a pivotal event in the dysfunctional homeostasis of neural membranes in the APP/PS1 mice, suggesting abnormalities in lipid rafts (Fabelo *et al.* 2012). In this study, a differential regulation of brain sphingomyelins was observed depending on the region considered and the fatty acid contained in the structure, as described for phospholipids. Thereby, saturated species were increased in hippocampus, and unsaturated ones decreased in cortex and cerebellum. However, the most important finding was the reduction of very long chain species in all brain regions investigated, in accordance with previous studies that demonstrated elevated degradation of sphingomyelins leading to the accumulation of ceramides containing very long chain fatty acids (Wang *et al.* 2008). On the other hand, reduced content of cholesterol has been already described in brains from transgenic mice of AD (Yao *et al.* 2009; Fabelo *et al.* 2012), generating serious alterations of the physicochemical structure of lipid rafts.

Finally, other discriminant metabolites could be considered as markers for integrity of the central nervous system, including deficits in dopamine and urea, as well as increased myo-inositol (Table 2). Dopamine is

a neurotransmitter derived from the amino acid tyrosine, commonly linked to Parkinson's disease, but whose reduction has been also reported in AD subjects (Storga *et al.* 1996). It is noteworthy that the higher decrease of this neurotransmitter was found in striatum, where dopaminergic neurons are primarily localized. The overall reduction in urea levels supports an abnormal homeostasis of ammonia in the whole brain, which may elicit deleterious effects on central nervous system (Felipo and Butterworth 2002). In this sense, the alteration of the urea cycle has been previously demonstrated on the basis of altered levels of expression in different enzymes and the corresponding genes (Hansmannel *et al.* 2001), which finally results in altered content of related metabolites (González-Domínguez *et al.* 2014b; González-Domínguez *et al.* 2015) as found in our metabolomic study. To conclude, the increase of myo-inositol has been traditionally proposed as a marker for osmotic stress or astrogliosis, frequently detected by ^{1}H-NMR investigations (Forster 2011; Woo *et al.* 2010).

In conclusion, this study shows that levels of numerous metabolites are altered in brain from APP/PS1 mice, such as phospholipids, amino acids or nucleotides among others, affecting primarily to hippocampus and cortex, and to a lesser extent cerebellum, striatum and olfactory bulbs. These metabolic alterations enabled the elucidation of underlying pathological mechanisms in the APP/PS1 mice, including abnormal metabolism of purines, bioenergetic failures, dyshomeostasis of amino acids and disturbances in membrane lipids. Furthermore, it is noteworthy the region-specificity of processes occurring in brain of the APP/PS1 mice. As a future plan, a second validation phase should be performed on a larger number of samples using a targeted approach, more sensitive and selective, in order to confirm our findings and demonstrate the potential of these discriminant metabolites as potential biomarkers for diagnosis.

Acknowledgements
This work was supported by the projects CTM2012-38720-C03-01 from the Ministerio de Ciencia e Innovación and P012-FQM-0442 and P009-FQM-4659 from the Consejería de Innovación, Ciencia y Empresa (Junta de Andalucía). Raúl González Domínguez thanks the Ministerio de Educación for a predoctoral scholarship.

References

Balayssac S., Déjean S., Lalande J., Gilard V., Malet-Martino M. (2013) A toolbox to explore NMR metabolomic data sets using the R environment. Chemometr. Intell. Lab. 126, 50-59.

Begley P., Francis-McIntyre S., Dunn W. B., Broadhurst D. I., Halsall A., Tseng A., Knowles J., HUSERMET Consortium, Goodacre R., Kell D. B. (2009) Development and performance of a gas chromatography-time-of-flight mass spectrometry analysis for large-scale nontargeted metabolomic studies of human serum. Anal. Chem. 81, 7038-7046.

Bollen E. and Prickaerts J. (2012) Phosphodiesterases in neurodegenerative disorders. IUBMB Life 64, 965-970.

Botosoa E. P., Zhu M., Marbeuf-Gueye C., Triba M. N., Dutheil F., Duyckäerts C., Beaune P., Loriot M. A., Le Moye L. (2012) NMR metabolomic of frontal cortex extracts: First study comparing two neurodegenerative diseases, Alzheimer disease and amyotrophic lateral sclerosis. IRBM 33, 281-286.

Braak H., Braak E., Bohl J., Lang W. (1989) Alzheimer's disease: amyloid plaques in the cerebellum. J. Neurol. Sci. 93, 277-287.

Braak H. and Braak E. (1991) Neuropathological stageing of Alzheimer-related changes. Acta Neuropathol. 82, 239-259.

Cai Z., Yan L. J., Li K., Quazi S. H., Zhao B. (2012) Roles of AMP-activated protein kinase in Alzheimer's disease. Neuromol. Med. 14, 1-14.

Chan R. B., Oliveira T. G., Cortes E. P., Honig L. S., Duff K. E., Small S. A., Wenk M. R., Shui G., Di Paolo G. (2012) Comparative lipidomic analysis of mouse and human brain with Alzheimer disease. J. Biol. Chem. 287, 2678-2688.

Chen S. Q., Cai Q., Shen Y. Y., Wang P. J., Teng G. J., Zhang W., Zang F. C. (2012) Age-related changes in brain metabolites and cognitive function in APP/PS1transgenic mice. Behav. Brain Res. 235, 1-6.

Czech C., Berndt P., Busch K., Schmitz O., Wiemer J., Most V., Hampel H., Kastler J., Senn H. (2012) Metabolite profiling of Alzheimer's disease cerebrospinal fluid. PLoS ONE 7, e31501.

Dedeoglu A., Choi J. K., Cormier K., Kowall N. W., Jenkins B. G. (2004) Magnetic resonance spectroscopic analysis of Alzheimer's disease mouse brain that express mutant human APP shows altered neurochemical profile. Brain Res. 1012, 60-65.

Domek-Lopacinska K. U. and Strosznajder J. B. (2010) Cyclic GMP and nitric oxide synthase in aging and Alzheimer's disease. Mol. Neurobiol. 41, 129-137.

Ellison D. W., Beal M. F., Martin J. B. (1987) Phosphoethanolamine and ethanolamine are decreased in Alzheimer's disease and Huntington's disease. Brain Res. 417, 389-392.
Fabelo N., Martín V., Marín R., Santpere G., Aso E., Ferrer I., Díaz M. (2012) Evidence for premature lipid raft aging in APP/PS1 double-transgenic mice, a model of familial Alzheimer disease. J. Neuropathol. Exp. Neurol. 71, 868-881.
Felipo V. and Butterworth R. F. (2002) Neurobiology of ammonia. Prog. Neurobiol. 67, 259-279.
Forster D. M., James M. F., Williams S. R. (2012) Effects of Alzheimer's disease transgenes on neurochemical expression in the mouse brain determined by ^{1}H MRS *in vitro*. NMR Biomed. 25, 52-58.
Frisardi V., Panza F., Seripa D., Farooqui T., Farooqui A. A. (2011) Glycerophospholipids and glycerophospholipid-derived lipid mediators: A complex meshwork in Alzheimer's disease pathology. Prog. Lipid Res. 50, 313-330.
Gonzalez-Dominguez R., Garcia-Barrera T., Gomez-Ariza J. L. (2014a) Combination of metabolomic and phospholipid-profiling approaches for the study of Alzheimer's disease. J. Proteomics 104, 37-47.
Gonzalez-Dominguez R., Garcia-Barrera T., Gomez-Ariza J. L. (2014b) Metabolomic study of lipids in serum for biomarker discovery in Alzheimer's disease using direct infusion mass spectrometry. J. Pharm. Biomed. Anal. 98, 321-326.
González-Domínguez R., Garcia-Barrera T., Gomez-Ariza J. L. (2015) Application of a novel metabolomic approach based on atmospheric pressure photoionization mass spectrometry using flow injection analysis for the study of Alzheimer's disease. Talanta 131, 480-489.
Graham S. F., Chevallier O. P., Roberts D., Holscher C., Elliot C. T., Green B. D. (2013a) Investigation of the human brain metabolome to identify potential markers for early diagnosis and therapeutic targets of Alzheimer's disease. Anal. Chem. 85, 1803-1811.
Graham S. F., Holscher C., McClean P., Elliott C. T., Green B. D. (2013b) ^{1}H NMR metabolomics investigation of an Alzheimer's disease (AD) mouse model pinpoints important biochemical disturbances in brain and plasma. Metabolomics 9, 974-983.
Hall A. M. and Roberson E. D. (2012) Mouse models of Alzheimer's disease. Brain Res. Bull. 88, 3-12.
Han X., Holtzman D. M., McKeel Jr D. W. (2001) Plasmalogen deficiency in early Alzheimer's disease subjects and in animal models: molecular characterization using electrospray ionization mass spectrometry. J. Neurochem. 77, 1168-1180.
Hansmannel F., Sillaire A., Kamboh M. I., Lendon C., Pasquier F., Hannequin D., Laumet G., Mounier A., Ayral A. M., DeKosky S. T., Hauw J. J., Berr C., Mann D., Amouyel P., Campion D., Lambert J. C. (2010) Is the urea cycle involved in Alzheimer's disease? J. Alzheimers Dis. 21, 1013-1021.
Hashimoto K., Fukushima T., Shimizu E., Okada S., Komatsu N., Okamura N., Koike K., Koizumi H., Kumakiri C., Imai K., Iyo M. (2004) Possible role of D-serine in the pathophysiology of Alzheimer's disease. Prog. Neuropsychopharmacol. Biol. Psychiatry 28, 385-388.
Haynes C. A., Allegood J. C., Park H., Sullards M. C. (2009) Sphingolipidomics: Methods for the comprehensive analysis of sphingolipids. J. Chromatogr. B Analyt. Technol. Biomed. Life Sci. 877, 2696-2708.
Hipkiss A. R. (2007) Could carnosine or related structures suppress Alzheimer's disease? J. Alzheimers Dis. 11, 229-240.
Hu Z. P., Browne E. R., Liu T., Angel T. E., Ho P. C., Chan E. C. Y. (2012) Metabonomic profiling of TASTPM transgenic alzheimer's disease mouse model. J. Proteome Res. 11, 5903-5913.
Ibáñez C., Simó C., Cifuentes A. (2013) Metabolomics in Alzheimer's disease research. Electrophoresis 34, 2799-2811.
Inoue K., Tsutsui H., Akatsu H., Hashizume Y., Matsukawa N., Yamamoto T., Toyo'oka T. (2013) Metabolic profiling of Alzheimer's disease brains. Sci. Rep. 3, 2364.
Jankowsky J. L., Fadale D. J., Anderson J., Xu G. M., Gonzales V., Jenkins N. A., Copeland N. G., Lee M. K., Younkin L. H., Wagner S. L., Younkin S. G., Borchelt D. R. (2004) Mutant presenilins specifically elevate the levels of the 42 residue beta-amyloid peptide in vivo: evidence for augmentation of a 42-specific g secretase. Hum. Mol. Genet. 13, 159-170.
Kaddurah-Daouk R., Rozen S., Matson W., Han X., Hulette C. M., Burke J. R., Doraiswamy P. M., Welsh-Bohmer K. A. (2011) Metabolomic changes in autopsy-confirmed Alzheimer's disease. Alzheimers Dement. 7, 309-317.
Kaddurah-Daouk R., Zhu H., Sharma S., Bogdanov M., Rozen S. G., Matson W., Oki N. O., Motsinger-Reif A. A., Churchill E., Lei Z., Appleby D., Kling M. A., Trojanowski J. Q., Doraiswamy P. M., Arnold S. E., Pharmacometabolomics Research Network (2013) Alterations in metabolic pathways and networks in Alzheimer's disease. Transl. Psychiatry 3, e244.
Kantarci K., Weigand S. D., Petersen R. C., Boeve B. F., Knopman D. S., Gunter J., Reyes D., Shiung M., O'Brien P. C., Smith G. E., Ivnik R. J., Tangalos E. G., Jack Jr C. R. (2007) Longitudinal ^{1}H

MRS changes in mild cognitive impairment and Alzheimer's disease. Neurobiol. Aging 28, 1330-1339.
Katajamaa M. and Oresic M. (2007) Data processing for mass spectrometry-based metabolomics. J. Chromatogr. A 1158, 318-328.
Kosicek M. and Hecimovic S. (2013) Phospholipids and Alzheimer's disease: Alterations, mechanisms and potential biomarkers. Int. J. Mol. Sci. 14, 1310-1322.
Lalande J., Halley H., Balayssac S., Gilard V., Déjean S., Martino R., Francés B., Lassalle J. M., Malet-Martino M. (2014) ^{1}H NMR metabolomic signatures in five brain regions of the AβPPswe Tg2576 mouse model of Alzheimer's disease at four ages. J. Alzheimers Dis. 39, 121-143.
Lee W. J., Hawkins R. A., Peterson D. R., Viña J. R. (1996) Role of oxoproline in the regulation of neutral amino acid transport across the blood-brain barrier. J. Biol. Chem. 271, 19129-19133.
Liang Z., Liu F., Grundke-Iqbal I., Iqbal K., Gong C. X. (2007) Down-regulation of cAMP-dependent protein kinase by over-activated calpain in Alzheimer disease brain. J. Neurochem. 103, 2462-2470.
Lin A. L., Laird, A. R., Fox, P. T., Gao, J. H. (2012) Multimodal MRI neuroimaging biomarkers for cognitive normal adults, amnestic mild cognitive impairment, and Alzheimer's disease. Neurol. Res. Int. 2012, 907409.
Lin S., Liu H., Kanawati B., Liu L., Dong J., Li M., Huang J., Schmitt-Kopplin P., Cai Z. (2013) Hippocampal metabolomics using ultrahigh-resolution mass spectrometry reveals neuroinflammation from Alzheimer's disease in CRND8 mice. Anal. Bioanal. Chem. 405, 5105-5117.
Lin S., Kanawati B., Liu L., Witting M., Li M., Huang J., Schmitt-Kopplin P., Cai Z. (2014) Ultra high resolution mass spectrometry-based metabolic characterization reveals cerebellum as a disturbed region in two animal models. Talanta 118, 45-53.
Lindon J. C., Holmes E., Nicholson J. K. (2004) Metabonomics and its role in drug development and disease diagnosis. Expert Rev. Mol. Diagn. 4, 189-199.
Llansola M., Sanchez-Perez A., Cauli O., Felipo V. (2005) Modulation of NMDA receptors in the cerebellum. 1. Properties of the NMDA receptor that modulate its function. Cerebellum 4, 154-161.
Maccioni R. B., Muñoz J. P., Barbeito L. (2001) The molecular bases of Alzheimer's disease and other neurodegenerative disorders. Arch. Med. Res. 32, 367-381.
Malm T., Koistinaho J., Kanninen K. (2011) Utilization of APPswe/PS1dE9 transgenic mice in research of Alzheimer's disease: Focus on gene therapy and cell-based therapy applications. Int. J. Alzheimers Dis. 2011, 517160.
Maruszak A. and Żekanowski C. (2011) Mitochondrial dysfunction and Alzheimer's disease. Prog. Neuropsychopharmacol. Biol. Psychiatry 35, 320-330.
Mosconi L., Mistur R., Switalski R., Tsui W. H., Glodzik L., Li Y., Pirraglia E., De Santi S., Reisberg B., Wisniewski T., de Leon M. J. (2009) FDG-PET changes in brain glucose metabolism from normal cognition to pathologically verified Alzheimer's disease. Eur. J. Nucl. Med. Mol. Imaging 36, 811-822.
Mota S. I., Ferreira I. L., Rego A. C. (2014) Dysfunctional synapse in Alzheimer's disease - A focus on NMDA receptors. Neuropharmacology 76, 16-26.
Nuutinen S. and Panula P. (2010) Histamine in neurotransmission and brain diseases. Adv. Exp. Med. Biol. 709, 95-107.
Piro J. R., Benjamin D. I., Duerr J. M., Pi Y. Q., Gonzales C., Wood K. M., Schwartz J. W., Nomura D. K., Samad T. A. (2012) A dysregulated endocannabinoid-eicosanoid network supports pathogenesis in a mouse model of Alzheimer's disease. Cell Rep. 1, 617-623.
Pulfer M. and Murphy R. C. (2003) Electrospray mass spectrometry of phospholipids. Mass Spectrom. Rev. 22, 332-364.
Redjems-Bennani N., Jeandel C., Lefebvre E., Blain H., Vidailhet M., Guéanta J. L. (1998) Abnormal substrate levels that depend upon mitochondrial function in cerebrospinal fluid from Alzheimer patients. Gerontology 44, 300-304.
Rowe C. C. and Villemagne V. L. (2013) Brain amyloid imaging. J. Nucl. Med. 41, 11-18.
Salek R. M., Xia J., Innes A., Sweatman B. C., Adalbert R., Randle S., McGowan E., Emson P. C., Griffin J. L. (2010) A metabolomic study of the CRND8 transgenic mouse model of Alzheimer's disease. Neurochem. Int. 56, 937-943.
Sangster T., Major H., Plumb R., Wilson A. J., Wilson I. D. (2006) A pragmatic and readily implemented quality control strategy for HPLC-MS and GC-MS-based metabonomic analysis. Analyst 131, 1075-1078.
Selkoe D. J. (2003) Folding proteins in fatal ways. Nature 426, 900-904.
Simic G., Stanić G., Mladinov M., Jovanov-Milosevic N., Kostovic I., Hof P. R. (2009) Does Alzheimer's disease begin in the brainstem? Neuropathol. Appl. Neurobiol. 35, 532-554.

Sims B., Powers R. E., Sabina R. L., Theibert A. B. (1998) Elevated adenosine monophosphate deaminase activity in Alzheimer's disease brain. Neurobiol. Aging 19, 385-391.
Smith C. A., Want E. J., O'Maille G., Abagyan R., Siuzdak G. (2006) XCMS: Processing mass spectrometry data for metabolite profiling using nonlinear peak alignment, matching, and identification. Anal. Chem. 78, 779-787.
Storga D., Vrecko K., Birkmayer J. G. D., Reibnegger G. (1996) Monoaminergic neurotransmitters, their precursors and metabolites in brains of Alzheimer patients. Neurosci. Lett. 203, 29-32.
Struble R. G. and Clark H. B. (1992) Olfactory bulb lesions in Alzheimer's disease. Neurobiol. Aging 13, 469-473.
Thauerer B., Zur Nedden S., Baier-Bitterlich G. (2012) Purine nucleosides: endogenous neuroprotectants in hypoxic brain. J. Neurochem. 121, 329-342.
Trushina E., Nemutlu E., Zhang S., Christensen T., Camp J., Mesa J., Siddiqui A., Tamura Y., Sesaki H., Wengenack T. M., Dzeja P. P., Poduslo J. F. (2012) Defects in mitochondrial dynamics and metabolomic signatures of evolving energetic stress in mouse models of familial Alzheimer's disease. PLoS ONE 7, e32737.
van den Berg R. A., Hoefsloot H. C. J., Westerhuis J. A., Smilde A. K., van der Werf M. J. (2006) Centering, scaling, and transformations: improving the biological information content of metabolomics data. BMC Genomics 7, 142.
Van Schaftingen E., Rzem R., Veiga-da-Cunha M. (2009) L: -2-Hydroxyglutaric aciduria, a disorder of metabolite repair. J. Inherit. Metab. Dis. 32, 135-142.
Veselkov K. A., Vingara L. K., Masson P., Robinette S. L., Want E., Li J. V., Barton R. H., Boursier-Neyret C., Walther B., Ebbels T. M., Pelczer I., Holmes E., Lindon J. C., Nicholson J. K. (2011) Optimized preprocessing of ultra-performance liquid chromatography/mass spectrometry urinary metabolic profiles for improved information recovery. Anal. Chem. 83, 5864-5872.
Walter A., Korth U., Hilgert M., Hartmann J., Weichel O., Hilgert M., Fassbender K., Schmitt A., Klein J. (2004) Glycerophosphocholine is elevated in cerebrospinal fluid of Alzheimer patients. Neurobiol. Aging 25, 1299-1303.
Wang C., Xie S., Yang J., Yang Q., Xu G. (2004) Structural identification of human blood phospholipids using liquid chromatography/quadrupole-linear ion trap mass spectrometry. Anal. Chim. Acta 525, 1-10.
Wang G., Silva J., Dasgupta S., Bieberich E. (2008) Long-chain ceramide is elevated in presenilin 1 (PS1M146V) mouse brain and induces apoptosis in PS1 astrocytes. Glia 56, 449-456.
Wang H., Lian K., Han B., Wang Y., Kuo S. H., Geng Y., Qiang J., Sun M., Wang M. (2014) Age-related alterations in the metabolic profile in the hippocampus of the senescence-accelerated mouse prone 8: a spontaneous Alzheimer's disease mouse model. J. Alzheimers Dis. 39, 841-848.
Woo D. C., Lee S. H., Lee D. W., Kim S. Y., Kim G. Y., Rhim H. S., Choi C. B., Kim H. Y., Lee C. U., Choe B. Y. (2010) Regional metabolic alteration of Alzheimer's disease in mouse brain expressing mutant human APP-PS1 by ^{1}H HR-MAS. Behav. Brain Res. 211, 125-131.
Yao J. K., Wengenack T. M., Curran G. L., Poduslo J. F. (2009) Reduced membrane lipids in the cortex of Alzheimer's disease transgenic mice. Neurochem. Res. 34, 102-108.

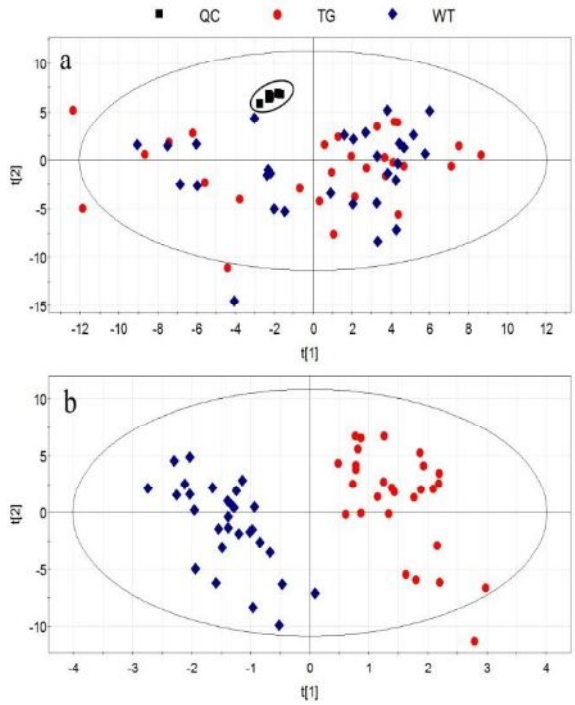

Fig. 1 Scores plots of PCA (A) and PLS-DA (B) models for hippocampus

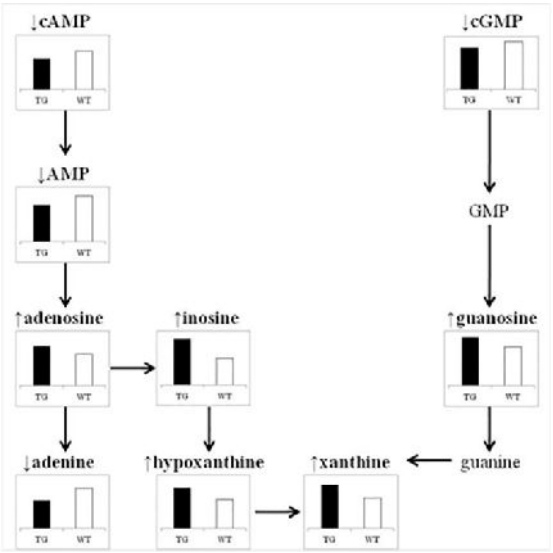

Fig. 2 Overview of hippocampal metabolomic changes in APP/PS1 mice related to purine metabolism

Table 1 Statistical parameters of PLS-DA models for hippocampus (HP), cortex (CT), striatum (ST), cerebellum (CB), and olfactory bulb (OB). A: number of latent components; R^2: variance explained; Q^2: variance predicted

		HP	CT	ST	CB	OB
GC/MS	**A**	4	4	3	3	3
	R^2	0.997	0.992	0.991	0.996	0.998
	Q^2	0.735	0.719	0.69	0.61	0.722
UPLC-ESI(+)/MS	**A**	4	4	5	5	6
	R^2	0.992	0.99	0.95	0.995	0.992
	Q^2	0.922	0.924	0.788	0.944	0.89
UPLC-ESI(-)/MS	**A**	5	4	6	6	7
	R^2	0.991	0.983	0.981	0.992	0.988
	Q^2	0.877	0.794	0.8	0.844	0.862

Table 2 Low molecular weight metabolites identified as potential markers for discrimination between APP/PS1 and control mice. HP, hippocampus; CT, cortex; ST, striatum; CB, cerebellum; OB, olfactory bulb. NS: non significant change

metabolite	RT (min)*	fold change				
		HP	CT	ST	CB	OB
amino acids						
glycine	4.42[a], 0.28[b]	0.72	0.62	0.74	1.47	NS
serine	4.72a, 0.28b	1.21	NS	1.35	NS	NS
threonine	4.95[a]	0.66	NS	NS	NS	NS
aspartate	6.07[a]	0.54	0.46	NS	NS	0.69
pyroglutamate	6.28[a], 0.28[b]	0.75	0.67	0.85	2.11	NS
glutamate	6.95[a], 0.28[b]	0.46	0.72	1.46	1.49	0.62
N-acetylaspartate	7.18[a]	0.75	0.46	1.58	1.22	0.72
valine	0.28[b]	1.14	1.07	1.10	NS	NS
histidine	0.28[b]	NS	0.71	NS	NS	NS
taurine	0.28[b]	0.92	0.92	0.73	0.85	NS
nucleotides						
adenine	0.32[b]	0.70	0.90	NS	NS	NS
hypoxanthine	8.47[a], 0.40[b]	1.41	1.46	1.46	1.53	NS
xanthine	9.85[a]	1.48	1.79	1.46	NS	NS
inosine	13.05[a], 0.42[b]	1.78	1.76	2.24	2.23	NS
adenosine	13.38[a]	1.21	1.35	NS	1.67	NS
guanosine	14.02[a]	1.24	1.24	1.58	1.47	NS
AMP	0.36[b]	0.80	0.89	0.82	NS	NS
cAMP	0.36[b]	0.79	0.84	0.82	NS	NS
cGMP	0.36[b]	0.87	NS	NS	NS	NS
UMP	0.36[b]	0.88	NS	NS	NS	NS
phosphoribosyl-AMP	0.36[b]	0.91	0.89	0.82	NS	NS
others						
lactic acid	2.70[a]	0.76	0.67	0.90	0.63	0.58
urea	3.97[a]	0.38	0.60	0.70	0.58	0.42
glycerol	4.08[a]	1.52	1.41	2.06	1.77	NS
malic acid	5.88[a]	0.78	0.65	NS	NS	NS
creatinine	6.38[a]	0.53	0.59	0.67	0.67	0.66
2-hydroxyglutarate	6.58[a]	NS	0.69	NS	0.58	NS
pyrophosphate	7.08[a]	0.84	NS	NS	NS	NS
ethanolamine	7.38[a]	0.53	0.45	0.69	0.82	0.48
glycerol-3-phosphate	7.97[a]	1.39	1.84	1.43	1.38	NS
citric acid	8.39[a]	0.45	0.61	0.69	0.73	NS
myoinositol	10.22[a]	2.11	1.37	1.82	2.07	1.34
glucose-6-phosphate	10.93[a]	0.67	NS	NS	NS	NS
cholesterol	16.47[a]	0.25	0.49	0.43	0.23	0.35
choline	0.28[b]	1.25	1.30	1.28	NS	NS
phosphocholine	0.28[b]	1.16	1.25	1.30	1.13	NS
glycerophosphocholine	0.28[b]	1.17	1.28	1.41	1.18	NS
dopamine	0.28[b]	0.94	NS	0.83	NS	NS
lactose	0.33[b]	1.18	NS	NS	NS	NS

** retention times for metabolites detected by GC/MS[a] and/or UPLC/MS[b]. Abbreviations: AMP, adenosine monophosphate; cAMP, cyclic adenosine monophosphate; cGMP, cyclic guanosine monophosphate; UMP, uridine monophosphate.*

Table 3 Lysophospholipids identified as potential markers for discrimination between APP/PS1 and control mice. HP, hippocampus; CT, cortex; ST, striatum; CB, cerebellum; OB, olfactory bulb. NS: non significant change

metabolite	RT (min)	fold change				
		HP	CT	ST	CB	OB
LPI(20:4)	4.07	1.56	1.60	1.67	NS	NS
LPE(22:6)	4.28	1.62	1.63	1.57	1.59	1.66

LPE(20:4)	4.28	1.79	1.72	1.35	NS	1.81
LPI(16:0)	4.32	1.53	NS	NS	NS	NS
LPC(22:6)	4.47	1.53	1.45	NS	NS	1.56
LPC(20:4)	4.47	1.46	1.61	1.61	NS	1.58
LPI(18:0)	4.87	1.62	1.84	NS	1.84	1.71
LPC(18:1)	4.88	1.54	1.38	NS	NS	1.61
LPI(20:1)	4.88	1.41	NS	NS	NS	NS
LPC(16:0)	4.93	1.28	1.36	1.67	NS	NS
LPE(18:0)	5.22	NS	1.49	NS	NS	NS
LPC(18:0)	5.67	1.36	1.56	1.74	1.56	NS

Abbreviations: LPI, lysophosphoinositol; LPE, lysophosphoethanolamine; LPC, lysophosphocholine.

Table 4 Phospholipids and sphingomyelins identified as potential markers for discrimination between APP/PS1 and control mice. HP, hippocampus; CT, cortex; ST, striatum; CB, cerebellum; OB, olfactory bulb. NS: non significant change

metabolite	**RT (min)**	**fold change**					**metabolite**	**RT (min)**	**fold change**				
		HP	**CT**	**ST**	**CB**	**OB**			**HP**	**CT**	**ST**	**CB**	**OB**
decreased phospholipids							**increased phospholipids**						
PC(18:3/22:6)	8.40	NS	0.67	0.66	NS	NS	PC(20:4/20:4)	8.17	NS	1.36	NS	NS	NS
PC(18:1/22:6)	8.46	NS	0.71	0.63	NS	0.66	PC(22:6/22:4)	8.40	1.46	1.39	NS	NS	NS
PC(18:0/22:6)	8.47	0.67	0.74	0.59	0.70	NS	PC(16:0/18:2)	8.57	1.61	1.80	1.55	1.80	1.43
PE(22:6/22:6)	7.68	0.68	NS	NS	NS	0.61	PC(18:0/20:4)	8.86	NS	1.36	NS	NS	NS
PE(16:1/20:4)	7.70	0.62	0.77	0.74	0.74	NS	PC(16:0/18:1)	8.87	NS	1.36	NS	NS	NS
PE(20:4/22:6)	7.73	0.68	NS	NS	NS	0.62	PC(18:1/18:0)	9.19	1.36	1.33	NS	NS	NS
PE(18:3/22:6)	7.97	NS	0.65	NS	NS	NS	PC(18:0/22:4)	9.20	NS	1.38	NS	NS	NS
PE(16:0/22:6)	7.97	NS	0.73	NS	0.73	0.66	PC(16:0/18:0)	9.25	NS	1.45	NS	NS	NS
PE(16:1/18:1)	8.02	0.70	NS	NS	0.75	NS	PE(20:4/20:4)	7.79	NS	1.32	NS	NS	NS
PE(18:1/20:4)	8.10	0.71	NS	NS	NS	0.64	PE(20:4/22:4)	8.11	NS	1.50	NS	1.39	NS
PE(16:0/18:1)	8.31	0.65	NS	NS	0.73	NS	PE(18:0/20:4)	8.40	NS	1.43	NS	NS	NS
PE(18:1/18:1)	8.40	0.63	0.66	0.70	0.77	0.72	PE(18:0/22:5)	8.58	NS	1.61	NS	NS	NS
PE(18:1/18:0)	8.66	0.72	NS	NS	NS	NS	PE(18:0/22:4)	8.66	1.43	1.62	NS	NS	NS
PPE(18:1/16:1)	8.20	0.62	0.66	NS	NS	NS	PPE(16:0/20:4)	8.20	NS	1.57	NS	NS	NS
PPE(18:1/20:4)	8.25	0.72	0.74	NS	NS	NS	PPE(18:0/20:4)	8.58	NS	1.42	NS	NS	NS
PPE(18:1/22:6)	8.25	NS	0.77	NS	NS	0.64	PPE(18:0/22:4)	8.85	NS	1.38	1.86	1.70	1.37
PPE(18:1/16:0)	8.49	0.68	NS	NS	NS	NS	PS(18:2/18:1)	7.97	1.33	NS	NS	NS	NS
PPE(18:1/18:1)	8.58	0.58	0.61	NS	NS	0.61	PS(18:0/22:5)	8.27	1.55	1.38	NS	NS	NS
PPE(18:0/18:1)	8.85	0.70	0.72	NS	0.72	NS	PS(18:0/20:4)	8.37	NS	1.62	NS	NS	NS
PPE(18:1/20:1)	8.92	0.71	NS	NS	NS	NS	PS(18:1/18:0)	8.37	NS	1.28	NS	NS	NS
PS(22:6/22:6)	7.35	0.71	0.77	0.63	NS	NS	PS(18:0/20:1)	8.67	1.33	NS	NS	NS	NS
PS(20:4/22:6)	7.40	0.50	NS	NS	NS	NS	PI(18:0/20:4)	7.94	NS	1.51	NS	NS	NS
PS(18:1/22:6)	7.74	0.67	NS	0.60	NS	NS	PG(18:0/20:4)	7.99	1.42	1.40	NS	NS	NS
PI(16:0/22:6)	7.51	NS	0.78	NS	NS	NS	PG(18:1/22:4)	8.01	1.37	NS	NS	NS	NS
PI(18:1/18:0)	8.22	0.68	NS	NS	NS	NS	SM(d18:1/16:0)	8.32	NS	1.37	NS	1.34	NS
PG(16:1/22:6)	7.35	0.73	0.68	NS	NS	NS	SM(d18:1/18:0)	8.70	NS	1.60	NS	1.55	NS
SM(d18:1/18:1)	8.38	0.67	NS	NS	NS	NS							
SM(d18:1/23:1)	9.55	0.63	0.69	NS	0.69	0.60							
SM(d18:1/24:1)	9.76	0.62	0.58	0.67	0.62	0.60							

Abbreviations: PC, phosphocholine; PE, phosphoethanolamine; PPE, plasmenylethanolamine; PS, phosphoserine; PI, phosphoinositol; PG, phosphoglycerol; SM, sphingomyelin.